Paper for *Electrochimica Acta* 2 July 2017

Characterisation of platinum electrodeposits on a titanium micromesh stack in a rectangular channel flow cell

Luis F. Arenas [a], Carlos Ponce de León [a], Richard P. Boardman [b], Frank C. Walsh [a,*]

[a] Electrochemical Engineering Laboratory, Energy Technology Group, Faculty of Engineering and the Environment, University of Southampton SO17 1BK, UK.

[b] μ-VIS X-ray Imaging Centre, Faculty of Engineering and the Environment, University of Southampton SO17 1BK, UK.

* Author for correspondence: F.C. Walsh; F.C.Walsh@soton.ac.uk

Abstract

Platinised titanium mesh is a common electrode material in industrial electrolytic cells and Ce-based redox flow batteries. In this work, the electrodeposition of platinum on a stack of titanium micromeshes is carried out from a flowing alkaline solution in a rectangular channel, divided flow cell. The morphology and distribution of platinum deposits are studied by SEM, EDS mapping and X-ray computer tomography. The active surface area of the electrode was assessed from the charge transfer current for the reduction of Ce(IV) and compared to that of planar and expanded metal mesh electrodes. The surface area was estimated by hydrogen electrosorption relative to that at a planar Pt/Ti electrode. As expected from the potential drop within the electrode channel, the individual micromesh near the cell separator displayed a higher platinum content. Pt/Ti micromesh offers an extended surface area and enhanced mass transport compared to planar electrodes and conventional expanded metal mesh anodes. The applications for these and alternative electrode structures are discussed.

Keywords: electroplating; flow cell; platinum; porous electrode; X-ray computed tomography.

(Approx. 7,400 words, 3 tables, 10 figures, 4 equations/reactions and 48 references).

1. Introduction

Due to their stability and electrocatalytic activity, platinised titanium (Pt/Ti) electrodes have found continued use, particularly as an anode, in electrochemical technology. Pt/Ti materials are commonly used in the electrolysis of inorganics, electrosynthesis of organic compounds, cathodic protection in sea water and as electroplating counter electrodes [1]. The most common form is the Pt/Ti expanded mesh, the titanium substrate typically being coated by electrodeposition in a stirred bath after the application of an iridium oxide interlayer by the 'dip/spay and bake' method [1].

Metal mesh electrodes can be stacked to form three dimensional (porous) electrodes for electrochemical flow cells and reactors. These electrodes can be implemented in the cells in flow-by, flow-through and flow-across configuration. Metal mesh is a widely available, cost-effective material having, usually, larger surface areas than plates or foils. Stacked mesh electrodes enhance mass transport [2,3] and flow dispersion [4], the effect being more pronounced with finer, rather than coarse or open varieties [5]. Furthermore, these structures have relatively high hydraulic permeability to flowing electrolytes [6,7], which decreases the pumping energy demand for electrolyte circulation compared to dense felt electrodes. The potential distribution and mass transfer characteristics of mesh electrodes in flow cells [8-10] as well as their residence time distribution [4] have been studied experimentally.

Currently, attention has been given to the enhancement of the conversion rate of cerium ions at Pt/Ti mesh electrodes in redox flow batteries (RFBs) [11-15] and other industrial electrochemical processes [16,17]. We have previously reported a quantitative analysis of the electrochemical performance of various three dimensional electrodes for the reduction of Ce(IV) ions in methanesulfonic acid solutions [3]. Evaluated electrode structures included Pt/Ti

plate, Pt/Ti mesh, Pt/Ti micromesh and Pt/Ti felt electrodes, the latter two being prepared in-house. The coating and resulting electroactive surface area of such electrodes were characterised. A study of the Pt/Ti felt electrode by several imaging techniques has already been reported [18].

This contribution describes the manufacture of Pt/Ti 'micromesh' electrodes, comprising their surface pre-treatment and subsequent electroplating in a rectangular channel flow cell. This alternative methodology to stirred baths was explored for convenience; a small volume of expensive solution can be easily recirculated in a flow cell. Also, in view of the possibility of preparing such electrodes in a single operation with complete coating of welding points, instead of the usual stacking of individually coated meshes. The suitability of the method is here established from the morphology and distribution of the platinum deposits on the micromesh stack. An indirect method was later employed to estimate the theoretical H electrosorption surface area.

Platinum electrodeposition from aqueous solutions can be performed in a number of ways [19,20]. In general, a planar geometry, such as an individual flat mesh, is electroplated in a stirred bath after a 'dip/spray and bake' treatment. Porous electrodes, such as titanium felt, are more difficult to coat uniformly in this manner, while chemical vapour deposition (CVD) and physical vapour deposition (PVD) tend to be too expensive for these applications and suffer from restricted sample size and line-of-sight restrictions. The controlled electrodeposition of Pt in flow cells has rarely been described [21,22], but is an important approach for some applications.

An additive-free alkaline electroplating bath was used for simplicity and to minimise hydrogen evolution compared to acidic chloride baths [19]. Since the predominant Pt(IV) species at pH 13 is $H_2Pt(OH)_6$ [23], the cathodic reduction to platinum metal is:

$$H_2Pt(OH)_6 + 4e^- \rightleftarrows Pt + 2H_2O + 4OH^- \quad (1)$$

A detailed discussion on the speciation of platinum, the parasitic hydrogen evolution and alternative reduction reactions has been provided in [18]. Commercially available plating baths based on stable complexes could have also been used to enhance grain refinement (typically for shiny coatings) and current efficiency. For instance, Pt(IV) tetrammine in a phosphate buffer [24].

2. Experimental details

2.1. Platinum electroplating solution

The electroplating solution had a composition of 20 g dm^{-3} (0.049 mol dm^{-3}) of hexachloroplatinic(IV) acid, H_2PtCl_6, in 0.1 mol dm^{-3} NaOH, according to a method described in [19]. The approximate mass fraction of Pt in the compound is 40% (Fischer Scientific Ltd., UK). Batches of 50 cm^3 were prepared at room temperature (22 °C) using deionized water as a solvent, yielding a stable, orange-coloured solution after several minutes of stirring. Chloride ions are substituted by hydroxyl ions when the Pt(IV) complex is present in alkaline media [23].

2.2. Flow cell and electrolyte recirculation

The rectangular channel flow cell employed for the electrodeposition of Pt on the Ti micromesh stack and its electrochemical performance have been described in previous work [3,18]. The two-compartment flow cell was made in acrylic polymer with the electrodes placed in a plane

parallel, flow-by configuration. Its components are shown in Figure 1. The Ti micromesh stack was the cathode in the negative half-cell, with a Pt/Ti plate as counter-electrode in the positive half-cell. Silicone rubber gaskets were placed between the components of the cell in order to provide hydraulic sealing under the compression applied by two plates fitted with bolts (not shown). Silicone sealant was used to fix the electrode into the acrylic back plate. As a means to form a flow channel with the same thickness as the porous electrode (S = 2.6 mm), the Nafion® 112 (Dupont Co, USA) ion exchange membrane was compressed against the micromesh stack with the help of three polypropylene meshes or inert 'turbulence promoters' (ITP) placed inside the positive half-cell, as shown in Figure 2b). The ITP meshes had a thickness of 1.3 mm and internal and external opening dimensions of 4.6 mm × 4.2 mm and 6.8 mm × 8.0 mm, respectively. A Luggin capillary was inserted through the cell frame to measure the electrode potential of the micromesh stack *vs*. a Hg|HgO reference electrode during the electrodeposition. Two Masterflex L/S (Cole-Parmer Co, USA) peristaltic pumps were used to recirculate the electroplating solution and the anolyte (0.1 mol dm^{-3} NaOH) through the negative and positive half-cells, respectively. These solutions were maintained in water jacketed reservoirs connected to a thermostatic water bath (Grant Instruments Ltd, UK). The cell was used in a three-electrode configuration and controlled by an Autolab digital potentiostat (Metrohm AG, The Netherlands).

2.3. Pt/Ti electrodes

As shown in Figure 2a), the Pt/Ti micromesh electrode was manufactured in-house and formed by a stack of sixteen flat titanium 'micromeshes' (Dexmet Co., USA) kept together by 9 welding spots on a 0.9 mm thick titanium plate (Alfa Aesar Ltd., UK). Its overall dimensions were 60 mm × 40 mm × 2.6 mm. As shown in Figure 2b), the individual micromeshes had dimensions of 60 mm × 22 mm, with a thickness of 170 μm, an internal aperture of 375 μm ×

625 μm and a pitch 670 μm × 1000 μm. The pieces of flat mesh were alternated with smaller 60 mm × 5 mm pieces of the same material at the opposite sides of the stack along the acrylic flow channel, to provide an adequate space for the flowing solution. Both the Pt/Ti plate and conventional Pt/Ti expanded mesh electrodes were sourced externally (Magneto BV, The Netherlands) and had a nominal Pt thickness of 3.5 μm. The planar electrode consisted of a 3 mm thick Ti plate coated with Pt on one side, while the Pt/Ti (coarse) mesh porous electrode consisted on three stacked meshes forming a volume 60 mm × 42 mm × 7.4 mm. The internal aperture of the mesh openings was approximately 3.2 mm × 7.1 mm, with a pitch of 6.8 mm × 10.1 mm and a thickness of 2.4 mm. Photographs of the external appearance of the electrodes can be found in [3]. The dimensions and hydraulic characteristics of the electrodes are given in Table 1.

2.4. Surface pre-treatment and electrodeposition

Prior to electrodeposition, the titanium micromesh stack was etched by passing a solution of 10% volume/weight of oxalic acid at 80 °C [25] through the single half-cell. For this, the electrolyte circuit was rearranged so that only one peristaltic pump was required; the other half-cell and membrane were temporarily removed. The oxalic acid solution was pumped for 2 hours until a dark brown solution appeared [25]. Oxalic acid can be used as an etchant and cleaner under conditions where excessive dissolution of titanium needs to be prevented, for instance, when using hot HCl [26].

Mass transport (and flow) can significantly influence the morphology and thickness of electroplated metals. At higher current densities, the reactant supply becomes rate limiting and thus convection will determine the deposit grow rate. This can be observed, e.g., in the electrodeposition of Pd at a planar electrode [27]. On the other hand, with already sufficient

mass transport and low current densities, the flow rate in cells with porous electrodes tends to have little effect on the electroplating rate, e.g., as shown by the concentration *vs*. time experiments in [28]. It is therefore necessary to report a mass transport related parameter to fully describe an electroplating environment.

After placing the Ti micromesh stack as the negative electrode, a 50 cm^3 volume of Pt(IV) solution was recirculated through this half-cell at a mean linear flow velocity of 8 cm s^{-1} ($v = Q/A_x\varepsilon$). This flow is equivalent to a channel Reynolds number ($Re = vd_e/\nu$) of approximately 710 (corresponding to laminar flow), where d_e is the equivalent hydraulic diameter of the rectangular flow channel, v is the mean linear electrolyte velocity and ν is the kinematic viscosity of the alkaline bath. In the positive half-cell, the 0.1 mol dm^{-3} NaOH supporting electrolyte was pumped at 8 cm s^{-1}. The solution temperature was kept at 75 °C. The composition of the electroplating bath and the electroplating environment are detailed in Table 2.

Platinum was electrodeposited at a constant potential of –0.2 V *vs.* $Hg|HgO_{(sat.)}$. During this operation, the colour of the plating solution became progressively less intense. Once the solution had become colourless, hydrogen evolution surged, indicating the complete removal of Pt(IV) from the solution. This was verified by a negative tin(II) chloride and potassium iodide spot tests on the residual electrolyte [29].

2.5. Study of coating morphology and distribution by imaging techniques

Scanning electron microscopy (SEM) and energy dispersive x-ray spectroscopy (EDS)

SEM images together with EDS spectra and maps of the Pt/Ti electrodes were acquired with a JSM-6500F field emission electron microscope (Jeol Inc, USA) and an INCA X-Sight energy

dispersive X-ray spectrometer (Oxford Instruments, U.K.), respectively. In order to study the Pt coating at the individual pieces of micromesh forming the Pt/Ti micromesh electrode, triangular samples of approximately 3.0 mm × 3.0 mm sides were taken from two of the corners of the electrode in the side closer to the electrolyte flow entrance; see Figure 2a). (The potential at these sites is not too dissimilar to that at the bulk mesh body when the fractional conversion is low [10,30,31].) In this way, sixteen pieces of the micromesh stack with different degrees of Pt coverage were obtained.

X-ray computed tomography (CT)

The samples taken from the Pt/Ti micromesh electrode were later used to reconstruct two stacks suitable for CT scanning to reveal the distribution of Pt across the stack between the planar current feeder and the membrane dividing the cell. One of the reconstructed stacks was taken from sections of the 1^{st}, 2^{nd}, 5^{th}, 8^{th}, and 16^{th} meshes, where the 1^{st} micromesh is adjacent to the membrane and the 16^{th} is adjacent to the current feeder. The second reconstructed stack formed the 1^{st} to the 8^{th} pieces of micromesh. The 4x objective of the Zeiss Xradia 510 Versa X-ray microscope 510 was used to perform the CT scans, yielding an isotropic resolution of 3.78 μm per voxel. The camera pixel binning was set to 2x, the X-ray peak voltage was 80 kV and the current was 87.5 μA, a 1.4 mm SiO_2 filter being applied. Each scan consisted of 1601 projections with an individual exposure time of 3 seconds. The distance from the source to the centre was 18 mm and 14 mm from the centre of the object to the detector. The resulting field of view was just under 3.8 mm. All CT images were processed in VGStudio MAX 2.1 CT visualisation suite (Volume Graphics GmbH, Germany).

2.6. Comparative electrochemical study of electrode surface area

As explained below, the charge transfer current for the reduction of Ce(IV) ions was recorded by linear sweep voltammetry at a small overpotential near the equilibrium potential with the aim of estimating the relative active surface area of the Pt/Ti micromesh compared to the Pt/Ti plate and conventional Pt/Ti mesh electrodes. The ratios of the charge transfer current were used for this purpose and later for the calculation of their theoretical H monolayer adsorption surface areas. The electrochemical performance of the same electrode materials in a Zn-Ce redox flow battery, expressed as the volumetric mass transport coefficient, $k_m A_e$, obtained from limiting current measurements (reduction of Ce(IV) ions), has been reported elsewhere [3]. The Pt/Ti micromesh yielded higher values than the Pt/Ti plate and the conventional Pt/Ti mesh, implying increased conversion rates and space time yield in the flow reactor. The Pt/Ti micromesh performance was, however, inferior to Pt/Ti felt electrodes.

Linear sweep voltammetry

The charge transfer current for ceric ion reduction at the Pt/Ti electrodes was determined from linear potential sweep voltammetry at 5 mV s^{-1} between potentials of –0.6 and +0.90 V *vs.* $Hg|Hg_2SO_{4(sat.)}$ at a temperature of 25 °C. In methanesulfonic acid [16]:

$$\mathrm{Ce(III)} - \mathrm{e}^- \rightleftarrows \mathrm{Ce(IV)} \qquad E^{\ominus} = +1.61\ \mathrm{V}\ \textit{vs.}\ \mathrm{SHE} \qquad (2)$$

An aqueous electrolyte for cerium-based redox flow batteries was employed, its composition being 0.1 mol dm^{-3} Ce(IV) methanesulfonate and 0.7 mol dm^{-3} Ce(III) methanesulfonate in 4.0 mol dm^{-3} methanesulfonic acid. The experimental arrangement has been described previously [3]. Measurements were taken at controlled electrolyte flow rates, from 0.5 cm s^{-1} to 17 cm s^{-1}. The concentration change in the 1.3 dm^3 of electrolyte during the experiments was < 3% at

the Pt/Ti micromesh electrode and negligible with the Pt/Ti mesh and plate electrodes, as shown by volumetric titration against a standard Fe(II) solution [32].

Hydrogen absorption

The active surface area of the planar Pt/Ti electrode was determined for monolayer hydrogen electrosorption in order to provide a baseline for the estimation of the Pt coverage at the Pt/Ti micromesh and Pt/Ti electrodes. A classical cyclic voltammetry technique considering a hydrogen monolayer charge density of 210 μC cm^{-2} in a deaerated 1.0 mol dm^{-1} H_2SO_4 solution [33] was employed. The linear potential sweep was carried out between –0.65 and +0.80 V *vs.* $Hg|Hg_2SO_{4(sat.)}$ at a rate of 1.0 V s^{-1} and a temperature of 25 °C. Given the relatively large dimensions of the Pt/Ti electrode, the three-electrode cell comprised a flanged glass tube with an internal diameter of 1.5 cm pressed into the plate and sealed with a silicone rubber gasket. The cell was fitted with a Nafion® 112 proton exchange membrane and a 1cm^2 Pt gauze counter-electrode. Three experiments were carried out at different sections of the electrode with approximate areas of 0.05 cm^2 and limited by an organic stop-off lacquer (Lacomit® Ltd, UK). These small representative sections of the Pt/Ti electrode were studied because the H electrosorption technique is unsuitable for large planar (24 cm^2 projected area) and macroporous (mesh, micromesh) electrodes due to their capacitive, uncompensated ohmic drop responses and difficulties determining the exact geometrical surface area.

3. Results and discussion

3.1. Platinum deposit morphology

The Pt/Ti micromesh after its electrodeposition and the externally sourced Pt/Ti mesh (for comparison) are shown in the SEM images in Figures 3a) and 3d). In the case of the Pt/Ti micromesh, the visible surface corresponds to the piece of micromesh nearest to the membrane

during electrodeposition, as seen in Figure 2b). The flow direction of the plating solution was perpendicular to the observed plane. The Pt/Ti micromesh shows a nearly uniform Pt coating populated by randomly distributed nodular structures of an approximate diameter of 60 μm. Meanwhile, the Pt/Ti mesh displays a homogeneous surface texture with a compact Pt coating. The microstructures Pt deposits at the Pt/Ti micromesh and Pt/Ti mesh are shown in Figures 3b) and 3e), respectively. Flattened Pt nodules with an approximate diameter of 5 μm cover the surface of the micromesh. This coating shows some degree of porosity, as revealed by the presence of crevices. Comparable Pt nodules have been obtained at a titanium micromesh coated with Pt-Ru by electrodeposition from a static solution of 5.0×10^{-3} mol dm^{-3} Pt(IV) in 0.1 mol dm^{-3} sulfuric acid [34]. The electrodeposition of a Pt-Ru catalyst on a titanium mesh produced a less uniform coating and showed higher porosity when performed in a solution containing 4.0×10^{-3} mol dm^{-3} Pt(IV) in 1.0 mol dm^{-3} sulfuric acid [35]. In contrast, the Pt coating at the Pt/Ti mesh shows overlapping Pt nodules of about 5 μm in diameter. The similarity of the dimensions of the nodular growths might be due to the nature of platinum nucleation during the electrochemical reduction of Pt(IV) ions.

Higher magnifications reveal that the type of Pt nucleation sites is different between the Pt/Ti micromesh and the commercially available Pt/Ti mesh. The Pt/Ti micromesh, shown in Figure 3c), involves the growth of spine growths under 0.2 μm long. On the other hand, the Pt/Ti mesh, shown in Figure 3f), consists of rounded protrusions with approximate dimensions of 0.1 μm; similar to those reported in [34]. These morphologies are quite different to the hemispherical nucleation sites obtained at carbon electrodes in HCl media [36], which are usually globular in shape.

Is it possible to modify the morphology of Pt at the micromesh using electroplating additives, alternative etching methods, different current densities and by ensuring a homogeneous potential across the electrodes. Smooth, compact coatings of noble metals on porous substrates have been achieved at relatively small electrodes in stirred or flowing baths, due to their practically uniform potential distribution. This is the case for a Ru/Ti felt in a sulfuric acid solution at 48 mA dm^{-2} [26], Pt/RVC in a phosphate buffer at 0.1 mA dm^{-2} [21], and Pd/RVC in hydrochloric acid solution under potentiostatic conditions [37].

3.2. Pt deposit composition and distribution

As shown in Figure 4, EDS spectra taken at the deposited metal and the substrate corroborate the presence of platinum on the titanium micromesh. EDS analysis was further used in order to assess the homogeneousness of platinum coverage at the micromesh electrode. Figure 5 displays SEM images and EDS elemental maps of the 1st, 8th and 16th micromeshes of the stack that comprises the Pt/Ti micromesh electrode. The 1st and 16th micromesh are adjacent to the membrane and negative current feeder, respectively. As seen in Figure 5b), nodular platinum growths are observed in the individual meshes close to the membrane, as shown in the SEM image of Figure 5a). However, the coverage is not entirely complete as shown by the EDS map for titanium in Figure 5c). The 8th mesh in the stack lies approximately in the middle of the electrode thickness and can be seen in Figure 5d). A relatively uniform platinum coverage is revealed by Figure 5e) in this site but Figure 5f) also shows that bare titanium surface is exposed throughout the mesh. The 16th mesh, which is immediately next to the negative current feeder, can be seen in Figure 5g). The platinum and titanium EDS maps in Figures 5h) and 5i), respectively, show that platinum is also electrodeposited in this site, partially covering the substrate. In summary, although the micromesh stack is covered with a thin, incomplete platinum film, nodules develop only in the mesh close to the membrane, where the potential

drop in the electrolyte phase (relative to that at the membrane) is low during the electrodeposition. The causes of this potential driven distribution of the deposits are discussed below. A similar heterogonous distribution of platinum was observed in a Pt/Ti felt electrode [18]. In this case, the platinum coated concentrated within a depth of approximately 200 μm next to the membrane, leaving the rest of the titanium felt only with traces of the noble metal.

3.3. Pt distribution within the micromesh as revealed by CT

The distribution of platinum in the Pt/Ti micromesh in the axis between the planar current feeder and the membrane was determined by X-ray CT imaging of two reconstructed stacks made with samples of the electrode. (Previous studies of metal deposits at porous electrodes using conventional X-ray imaging and low-resolution CT in electrochemical flow cells can be found in the literature [38-40].) Figure 6a) shows a reconstructed Pt/Ti micromesh electrode formed by a stack of representative individual pieces of the original electrode embedded in epoxy resin. The reconstruction was required for the CT analysis because the only relatively small objects can be imaged with high resolution and because the stack was formed by independent pieces of micromesh. Figure 6b) confirms that most of the platinum is deposited on the top of the electrode sample, in the section farthest from the counter electrode and closest to the ion exchange membrane during electrodeposition. Only a few platinum nodules, marked in bright blue in the figure, can be observed through the thickness of the electrode and close to the current feeder. The platinum deposit appears to completely cover the 1st mesh next to the membrane, as seen in its cross-sectional image in Figure 7a). The maximum thickness of the observed platinum layer is approximately 36 μm. In contrast, the 16th mesh observed in Figure 7b) displays no indication of a platinum layer but a dispersion of nodules between 15 μm and 50 μm in diameter. A cross-section of another reconstructed electrode is shown in Figure 8. A platinum coating is clearly visible in the first layer of micromesh next to the membrane. The

micromeshes below do not display coatings of any significant thickness at this resolution, although platinum nodules are observed throughout them. This suggests that platinum deposits develop on places where the nucleation potential was high at the beginning of the electrodeposition, such as in local impurities of the material.

Both the Pt/Ti micromesh and Pt/Ti mesh electrodes have been implemented successfully in a Zn-Ce RFB unit flow cell, where their average volumetric mass transport coefficients, $k_m A_e$, were determined via the limiting current technique [3]. Maximum limiting current enhancement factors of 63 and 20 were displayed by the micromesh and mesh for cerium conversion, respectively, in comparison to a planar Pt/Ti electrode in an unrestricted flow channel. More significantly, the Pt/Ti micromesh developed $k_m A_e$ values comparable to partially-coated titanium felt and nearly one order of magnitude superior to the Pt/Ti mesh discussed in this work. However, total homogeneous coatings are desirable in practical applications. Furthermore, the advantages of finer Pt/Ti mesh electrodes over coarser ones have also been noted in H_2-Ce RFBs [15], where they showed an extension of the mass transport limitations at a higher operational current density. This type of titanium-based electrode must be fully covered with Pt in order to ensure their stability in RFBs and to prevent cathodic corrosion of the exposed Ti (due to hydrogen adsorption and brittle hydride formation) if used for H_2 evolution. For the several industrial applications where these electrodes operate exclusively as anodes [16], the partially coated Pt/Ti micromesh might be more stable, due to the passivation of titanium by a TiO_2 layer.

3.4. Effects of potential distribution on Pt electrodeposition

The heterogeneous distribution of the electrodeposited platinum is a result of the potential drop within the electrolyte phase permeating the micromesh electrode between the membrane

separator and the current feeder/collector [41]; the Ohmic drop through the metallic electrode material is negligible in comparison. The individual pieces of micromesh adjacent to the membrane in the cathodic compartment experience a significantly higher potential than those next to the current feeder in flow-by configuration [41]. (This effect is less severe when the reactant conversion per pass along the porous electrode is high [42,43].) This also means that the potential becomes more negative towards the current feeder and closer to that of H_2 evolution. As a result, the nucleation of platinum is enhanced at the start of the electrodeposition process near the membrane. Since platinum electrodeposition is notoriously susceptible to overpotential nucleation [36], the deposits continue to grow on these sites during the remainder of the reaction in the characteristic form of hemispherical nodules. Although some platinum electrodeposition is observed near the current feeder, as seen Figure 5h) and Figure 7b), the fact that its transversal distribution (Y axis in the cell) is highly concentrated at the planes near the membrane (see Figure 6) confirms the effects of overpotential nucleation.

The Ohmic drop taking place through the electrolyte phase across the thickness (Y axis in Figure 2) of an stacked mesh electrode at the entrance plane of a rectangular flow channel is given by [30,31,41,44]:

$$E_{(S)} - E_{(C)} = \Delta E = \frac{k_m A_e z F c_{in} S^2}{2\kappa} \qquad (3)$$

Where $E_{(S)}$ is the potential near the separator (membrane), at the distance S from the current feeder/collector (thickness of porous electrode channel), $E_{(C)}$ is the potential at the planar current feeder/collector, z is the electron stoichiometry, F is Faraday's constant, c_{in} is the inlet concentration of the reactant and κ is the electrolyte's conductivity. The model is valid for a mass transport controlled reaction regime. The resulting potential drop, ΔE, gives a good

approximation of that taking place across the length of the electrode at low fractional conversion [10,30,31]. Due to a limited supply of reagent, the measurement of $k_m A_e$ and κ for the electrodeposition of platinum at the micromesh stack was not accessible to us. In lieu, we present in Figure 9 the estimated ΔE across the electrolyte at the Pt/Ti micromesh electrode for the reduction of Ce(IV) ions in the same flow cell at a mean linear electrolyte velocity of 4 cm s^{-1}. In these conditions, $k_m A_e$ is 0.055 s^{-1} for the micromesh electrode [3]. An electrolyte concentration of 0.4 mol dm^{-3} Ce(IV) and a conductivity of 375 mS cm^{-1} were considered [45]. As seen in the Figure 9, ΔE increases exponentially with increasing electrode thickness (number of stacked pieces of mesh), reaching 1.0 V at approximately 1.9 mm. A similar trend occurs during the electrodeposition of platinum at the titanium micromesh substrate, resulting in the observed heterogeneous distribution of the deposit. The Pt/Ti mesh and Pt/Ti plate for the Ce reaction are shown for comparison. Electrode materials with low $k_m A_e$ values result in less severe potential drops.

The effects of potential drop on the electrodeposition of metals at other porous electrodes in rectangular channel flow cells and their study by conventional X-ray imaging and X-ray CT have been reported before. For instance, in a related work on the electrodeposition of platinum on a porous titanium felt [18] and earlier in the preparation of a RVC/Pt amperometric glucose sensor [21]. In the latter case, the platinum deposited mostly near the counter-electrode in the undivided, flow-through cell. Other cases involve the electrodeposition of zinc on RVC at the negative electrode of a Zn-Br flow battery [46] and in a flow reactor for zinc removal in acidic chloride solutions [28]. In both examples, the metal deposited near the positive electrode at a maximum depth of approximately 1.5 mm with negligible effect of mass transport at the evaluated electrolyte flow rates.

These findings imply that uniform metal coatings can only be achieved effectively at thin porous electrodes when electrodeposition is performed in parallel plate electrochemical flow cells. The possibilities for this manufacture technique could be expanded by performing the electrodeposition of mesh electrodes between parallel plate anodes and by employing suitable electroplating additives to promote nucleation or electrolytes with high conductivity. Pulse electrodeposition might also improve the uniformity of metal deposition on porous materials [47]. In the case of platinum, electroless deposition [20] and chemical vapour deposition [48] are a more appropriate choice to achieve homogeneous deposits on highly porous electrode materials, such as felts.

3.5. Comparative assessment of electrode active surface area

An approximation of the active electrode area, A_a, of the Pt/Ti micromesh and Pt/Ti mesh has been obtained from the current measured at the charge-transfer region, I_{CT}, during linear sweep voltammetry at a specific overpotential value from the open circuit potential (-20 mV) for a reaction of interest, i.e., the reduction of Ce(IV) ions. In this region, the current is proportional to the active electrode area, A_a, and expressed by:

$$I_{CT} = zFA_a kc \exp(\alpha zF\eta/RT) \quad (4)$$

Assuming full charge-transfer control and similar reaction kinetics, the A_a values of porous electrodes can be estimated from the I_{CT} ratios in respect to a planar electrode at the same temperature. Such ratios are here denominated Ψ. In this region of the polarization curve, convective diffusion should have a negligible contribution to the measured current [49].

The values of I_{CT} for the different electrodes obtained from the polarization curves for the reduction of Ce(IV) ions performed in a flow cell, shown in Figure 10, and the resulting charge-

transfer current ratios Ψ at -20 mV from the open circuit potential are given in Table 3. The standard deviation for the current values and the average open-circuit potential were calculated from 4 measurements. According to their Ψ values, the available Pt surface area in this Pt/Ti micromesh is 8.4 times that of a Pt/Ti plate and 1.75 times larger than that of the Pt/Ti mesh. In turn, Ψ is 4.8 in the case of the Pt/Ti mesh, which is a reasonable value for expanded metal.

The real surface area of platinum is commonly measured by the classical charge to area-relationship for the electrosorption of a H monolayer in 1.0 mol dm^{-3} sulfuric acid [33]. Therefore, the charge-transfer current ratios have been further employed to extrapolate the theoretical A_a of the porous electrodes for H electrosorption from the knowledge of the experimentally measured A_a of a Pt/Ti plate electrode. It is assumed that the charge for electrosorption keeps the same proportionality observed for the reduction of Ce(IV) ions, as it depends directly on the available Pt surface. The known area of the Pt/Ti electrode is 748.8±16.8 cm^2, as indicated by multiplying its geometrical area (24 cm^2) by the average roughness factor (31.2±0.7) determined by voltammetry at the sample sections of the plate; see the experimental section. One of the voltammograms showing the characteristic absorption and desorption peaks for the H monolayer at the Pt/Ti planar electrode has been reported in a related work [18].

The extrapolated values of A_a for the Pt/Ti micromesh and Pt/Ti mesh electrodes are presented in Table 3 as ≈ 6,800 cm^2 and ≈ 3,600 cm^2, respectively. A comparable proportion of 2 to 1 was noted between the surface areas of coarse and fine expanded Ti mesh [5]. A normalised figure considering the different overall volumes of the electrodes in the rectangular channel of the flow cell has also been calculated. The volumetric active platinum areas of the Pt/Ti micromesh and Pt/Ti mesh are thus ≈ 1,010 cm^{-1} and ≈ 190 cm^{-1}, respectively. Clearly, the micromesh

offers a significant increase of active electrode area, even with an incomplete coating. Such values are consistent with almost one order of magnitude difference in the $k_m A_e$ coefficients displayed by these electrodes in [3].

Several factors contribute to the error in the extrapolated surface area of the Pt/Ti mesh stacks, including the surface area of the planar electrode and the exponential effect of η. The relative error for I_{CT} at the micromesh and mesh is 2% and 21%, respectively, due to the variation in the linear sweep experiments. Uncertainties in the calculation of the electrochemical active surface area of large-size electrodes in electrochemical reactors are common, in contrast to, e.g., small disc electrodes in three-electrode cells. For example, a method based on the voltammetric measurement of capacitance at planar carbon polymer-based electrodes in redox flow batteries has yielded accuracies of about 20% [50]. As a result, the product $k_m A_e$ is frequently employed as a normalised performance factor in comparative and scale-up studies of electrochemical flow reactors [44].

4. Conclusions

- Pt/Ti porous electrodes can be prepared by potentiostatic electrodeposition in alkaline media employing divided rectangular channel flow cells. However, the potential drop at the electrolyte flooding the porous materials limits the thickness that can be effectively coated by this method. In the case stacks of fine mesh, the individual piece facing the separator or the anode will be electroplated preferentially. It may be advantageous to construct such electrodes with pre-coated pieces of mesh.
- It is possible to estimate the active surface area of porous electrodes from the ratio of the charge-transfer current relative to a planar electrode. The resulting error depends on

accuracy and reproducibility of the considered overpotential and measured current as well as on the area of the planar electrode and similar electrode kinetics.

- The electrochemical active surface area Pt/Ti micromesh is superior to that of conventional Pt/Ti mesh and Pt/Ti plates and can be favourably employed in electrochemical flow reactors, augmenting their limiting current, space time yield, and fractional conversion rate. Some potential applications are: RFBs, electrolysers, fuel cells and filter-press reactors for removal of metal ions, destruction of organics and manufacture of chemicals.
- Uniform coatings at mesh electrodes in flow cells can be obtained more effectively by electrodeposition between two parallel counter-electrodes. Alternatively, whole mesh stacks could be coated by electroless deposition or CVD, albeit at higher cost.

Acknowledgements

LFA acknowledges the support of CONACYT [scholarship 314057, 2013] and SEP [grant BC-1308, 2016] as well as the additional materials supplied by the Research Institute for Industry of the University of Southampton. The authors acknowledge collaboration with the μ-VIS centre at the University of Southampton for provision of tomographic imaging facilities, supported by EPSRC [grant EP-H01506X, 2009].

References

[1] G.K. Chandler, J.D. Genders, D. Pletcher, Electrodes based on noble metals, Platinum Metals Rev. 41 (1997) 54–63.

[2] C.J. Brown, D. Pletcher, F.C. Walsh, J.K. Hammond, D. Robinson, Studies of three-dimensional electrodes in the FMO1-LC laboratory electrolyser, J. Appl. Electrochem. 24 (1994) 95–106.

[3] L.F. Arenas, C. Ponce de León, F.C. Walsh, Mass transport and active area of porous Pt/Ti electrodes for the Zn-Ce redox flow battery determined from limiting current measurements, Electrochim. Acta. 221 (2016) 154–166.

[4] F.F. Rivera, M.R. Cruz-Díaz, E.P. Rivero, I. González, Analysis and interpretation of residence time distribution experimental curves in FM01-LC reactor using axial dispersion and plug dispersion exchange models with closed–closed boundary conditions, Electrochim. Acta. 56 (2010) 361–371.

[5] L. Lipp, D. Pletcher, Extended area electrodes based on stacked expanded titanium meshes, Electrochim. Acta. 42 (1997) 1101–1111.

[6] C.J. Brown, F.C. Walsh, D. Pletcher, Mass transfer and pressure drop in a laboratory filterpress electrolyser, Trans. IChemE. 73 (1995) 196–205.

[7] L.F. Arenas, C. Ponce de León, F.C. Walsh, Pressure drop through platinised titanium porous electrodes for cerium-based redox flow batteries, *submitted*.

[8] F. Leroux, F. Coeuret, Mass transfer and potential distribution within axial flow-through electrodes of expanded metal, Electrochim. Acta. 28 (1983) 1857–1863.

[9] F. Leroux, F. Coeuret, Flow-by electrodes of ordered sheets of expanded metal—I. Mass transfer and current distribution, Electrochim. Acta. 30 (1985) 159–165.

[10] F. Leroux, F. Coeuret, Flow-by electrodes of ordered sheets of expanded metal—II. Potential distribution for the diffusional regime, Electrochim. Acta. 30 (1985) 167–172.

[11] P.K. Leung, C. Ponce de León, C.T.J. Low, A.A. Shah, F.C. Walsh, Characterization of a zinc-cerium flow battery, J. Power Sources. 196 (2011) 5174–5185.

[12] P.K. Leung, C. Ponce de León, F.C. Walsh, An undivided zinc–cerium redox flow battery operating at room temperature (295 K), Electrochem. Commun. 13 (2011) 770–773.

[13] F.C. Walsh, C. Ponce de León, L. Berlouis, G. Nikiforidis, L.F. Arenas-Martínez, D. Hodgson, et al., The development of Zn-Ce hybrid redox flow batteries for energy storage and their continuing challenges, ChemPlusChem. 80 (2015) 288–311.

[14] H.M.H. Dewage, B. Wu, A. Tsoi, V. Yufit, G.J. Offer, N. Brandon, A novel regenerative hydrogen cerium fuel cell for energy storage applications, J. Mater. Chem. A. 3 (2015) 9446–9450.

[15] M.C. Tucker, A. Weiss, A.Z. Weber, Improvement and analysis of the hydrogen-cerium redox flow cell, J. Power Sources. 327 (2016) 591–598.

[16] L.F. Arenas, C. Ponce de León, F.C. Walsh, Electrochemical redox processes involving soluble cerium species, Electrochim. Acta. 205 (2016) 226–247.

[17] R. Roussel, C. Oloman, S. Harrison, Redox Mediated In-Cell Electrosynthesis of p-

anisaldehyde, J. Electrochem. Soc. 163 (2016) E414–E420.

[18] L.F. Arenas, C. Ponce de León, R.P. Boardman, F.C. Walsh, Electrodeposition of platinum on titanium felt in a rectangular channel flow cell, J. Electrochem. Soc. 164 (2017) D57–D66.

[19] M.E. Baumgärter, C.J. Raub, The electrodeposition of platinum and platinum alloys, Platinum Metals Rev. 32 (1988) 188–197.

[20] C.R.K. Rao, D.C. Trivedi, Chemical and electrochemical depositions of platinum group metals and their applications, Coord. Chem. Rev. 249 (2005) 613–631.

[21] G.H. Heider, S.V. Sasso, K. Huang, A.M. Yacynych, H.J. Wieck, Electrochemical platinization of reticulated vitreous carbon electrodes to increase biosensor response, Anal. Chem. 62 (1990) 1106–1110.

[22] U.M. López-García, P.E. Hidalgo, J.C. Olvera, F. Castañeda, H. Ruiz, G. Orozco, The hydrodynamic behavior of a parallel-plate electrochemical reactor, Fuel. 110 (2013) 162–170.

[23] P. Patnaik, Handbook of Inorganic Chemicals, McGraw-Hill, New York, 2003.

[24] A.J. Gregory, W. Levason, R.E. Noftle, R. Le Penven, D. Pletcher, Studies of platinum electroplating baths Part III. The electrochemistry of $Pt(NH_3)_{4-x}(H_2O)^{2+}_x$ and $PtCl_{4-x}(H_2O)^{(2-x)-}_x$, J. Electroanal. Chem. 399 (1995) 105–113.

[25] C.H. Angell, Surface treatment of titanium, US Patent 3,650,861, 1972.

[26] K. Kugler, M. Luhn, J.A. Schramm, K. Rahimi, M. Wessling, Galvanic deposition of Rh and Ru on randomly structured Ti felts for the electrochemical NH_3 synthesis, Phys. Chem. Chem. Phys. 17 (2015) 3768–3782.

[27] J.E. Terrazas-Rodríguez, S. Gutiérrez-Granados, M.A. Alatorre-Ordaz, C. Ponce de León, F.C. Walsh, A comparison of the electrochemical recovery of palladium using a parallel flat plate flow-by reactor and a rotating cylinder electrode reactor, Electrochim. Acta. 56 (2011) 9357–9363.

[28] M.R.V. Lanza, R. Bertazzoli, Removal of Zn(II) from chloride medium using a porous electrode: current penetration within the cathode, J. Appl. Electrochem. 30 (2000) 61–70.

[29] F. Feigl, V. Anger, Spot Tests in Inorganic Analysis, 6 ed., Elsevier, Amsterdam, 2012.

[30] F. Coeuret, A. Storck, Eléments de Génie Électrochimique, 2nd ed., Éditions TEC et DOC / Lavoisier, 1993.

[31] F. Coeuret, Introducción a la Ingeniería Electroquímica, Editorial Reverté, Barcelona, 1992.

[32] P. Trinidad, C. Ponce de León, F.C. Walsh, The use of electrolyte redox potential to monitor the Ce(IV)/Ce(III) couple, J. Environ. Manage. 88 (2008) 1417–1425.

[33] S. Trasatti, O.A. Petrii, Real surface area measurements in electrochemistry, Pure Appl. Chem. 63 (1991) 711–734.

[34] M.I. Awad, M.M. Saleh, T. Ohsaka, Ozone electrogeneration on Pt-loaded reticulated vitreous carbon using flooded and flow-through assembly, J. Electrochem. Soc. 153 (2006) D207–D212.

[35] R.G. Allen, C. Lim, L.X. Yang, K. Scott, S. Roy, Novel anode structure for the direct methanol fuel cell, J. Power Sources. 143 (2005) 142–149.

[36] H.M. Yasin, G. Denuault, D. Pletcher, Studies of the electrodeposition of platinum metal from a hexachloroplatinic acid bath, J. Electroanal. Chem. 633 (2009) 327–332.

[37] M. Łukaszewski, A. Żurowski, A. Czerwiński, Hydrogen in thin Pd-based layers deposited on reticulated vitreous carbon—A new system for electrochemical capacitors, J. Power Sources. 185 (2008) 1598–1604.

[38] Z. Fishman, J. Hinebaugh, A. Bazylak, Microscale tomography investigations of heterogeneous porosity distributions of PEMFC GDLs, J. Electrochem. Soc. 157 (2010) B1643–B1650.

[39] G. Qiu, C.R. Dennison, K.W. Knehr, E.C. Kumbur, Y. Sun, Pore-scale analysis of effects of electrode morphology and electrolyte flow conditions on performance of vanadium redox flow batteries, J. Power Sources. 219 (2012) 223–234.

[40] O.G. Olvera, G.T. Lapidus-Lavine, Use of X-ray tomography for the experimental verification of a mathematical model for the recovery of Cu and Cd in a flow-by porous electrode reactor, Int. J. Chem. React. Eng. 10 (2012) article A36.

[41] S. Langlois, F. Coeuret, Flow-through and flow-by porous electrodes of nickel foam Part III: theoretical electrode potential distribution in the flow-by configuration, J. Appl. Electrochem. 20 (1990) 740–748.

[42] A.I. Masliy, N.P. Poddubny, A.Z. Medvedev, V.O. Lukyanov, Analysis of the distribution of geometrical current density along the direction of solution flow inside flow-by porous electrodes, J. Electroanal. Chem. 757 (2015) 128–136.

[43] A.I. Maslii, N.P. Poddubnyi, A.Z. Medvedev, Distribution of geometrical current density inside a flow-by porous electrode: Effect of electrode parameters and electrochemical reactions, Russ. J. Electrochem. 52 (2016) 576–583.

[44] F.C. Walsh, A First Course in Electrochemical Engineering, The Electrochemical Consultancy, Romsey, 1993.

[45] L.F. Arenas, F.C. Walsh, C. Ponce de León, The importance of cell geometry and electrolyte properties to the cell potential of Zn-Ce hybrid flow batteries, J. Electrochem. Soc. 163 (2016) A5170–A5179.

[46] C.D. Iacovangelo, F.G. Will, Parametric study of zinc deposition on porous carbon in a flowing electrolyte cell, J. Electrochem. Soc. 132 (1985) 851–857.

[47] M.S. Chandrasekar, M. Pushpavanam, Pulse and pulse reverse plating—Conceptual, advantages and applications, Electrochim. Acta. 53 (2008) 3313–3322.

[48] M.J. Rand, Chemical vapor deposition of thin-film platinum, J. Electrochem. Soc. 120 (1973) 686–693.

[49] R. Guidelli, R.G. Compton, J.M. Feliu, E. Gileadi, J. Lipkowski, W. Schmickler, et al., Defining the transfer coefficient in electrochemistry: An assessment (IUPAC Technical Report), Pure Appl. Chem. 86 (2014) 245–258.

[50] N.J. Magnani, R.P. Clark, J.W. Braithwaite, D.M. Bush, Butler, P. C., J.M. Freese, et al., Exploratory battery technology development and testing report for 1985 SAND86-1266, Sandia National Laboratories, 1987.

Nomenclature

A Geometrical electrode area, (cm^2)

A_a Active electrode area, (cm^2)

A_e Volumetric active electrode area, (cm^{-1})

A_x Cross-sectional surface area of flow channel, (cm^2)

B Breadth of a rectangular flow channel, (cm)

c Reactant concentration, (mol dm^{-3})

c_{in} Reactant concentration at the inlet of a rectangular channel flow cell, (mol dm^{-3})

d_e Equivalent diameter of flow channel *(*$d_e = 2BS/(B+S)$*)*, (cm)

E_0 Equilibrium potential, (V)

$E_{(S)}$ Electrolyte potential near the separator, (V)

$E_{(C)}$ Electrolyte potential near the current feeder/collector, (V)

F Faraday constant, (C mol^{-1})

I_{CT} Charge transfer current, (A)

k Electron transfer rate, (cm^3 mol^{-1} cm^{-1})

k_m Mass transport coefficient, (cm s^{-1})

$k_m A_e$ Volumetric mass transport coefficient, (s^{-1})

L Length of a rectangular flow channel, (cm)

Q Volumetric flow rate, (cm^3 s^{-1})

R Molar gas constant, (J K^{-1} mol^{-1})

Re Reynolds number *(*$Re = vd_e/\nu$*),* (dimensionless)

S Height of a rectangular flow channel = overall porous electrode stack thickness, (cm)

T Temperature, (°C)

v Mean linear flow velocity past the electrode surface, (cm s^{-1})

z Electron stoichiometry, (dimensionless)

α Charge transfer coefficient, (dimensionless)

ΔE Potential drop within the electrolyte phase, (V)

ε Volumetric porosity, (dimensionless)

η Overpotential, (V)

κ Ionic conductivity, (S cm^{-1})

ν Kinematic viscosity of fluid, (cm^2 s^{-1})

Ψ Current ratio to planar electrode, (dimensionless)

Abbreviations

CT X-ray computed tomography

CVD Chemical vapour deposition

BET Brunauer–Emmett–Teller gas adsorption theory

DSA Dimensionally stable anodes

EDS Energy-dispersive X-ray spectroscopy

ITP Inert turbulence promoter

Pt/Ti Platinised titanium

PVD Physical vapour deposition

RFB Redox flow battery

SEM Scanning electron microscopy

SOC State of charge

Table 1. Characteristics of the Pt/Ti electrodes in a rectangular channel flow cell.

Electrode	Origin	Volumetric porosity, ε	Length, L / cm	Breadth, B / cm	Height, S / cm	Equivalent hydraulic diameter, d_e / cm
Pt/Ti plate + ITP	Supplied	0.78	6.0	4.0	0.36	0.65
Pt/Ti mesh	Supplied	0.71	6.0	4.2	0.74	1.26
Pt/Ti micromesh	In-house	0.53	6.0	4.0	0.26	0.48

Table 2. Composition of the electroplating bath and reaction environment during the electrodeposition of platinum on the titanium micromesh stack.

Property	Value
Hexachloroplatinic(IV) acid concentration	20 g dm^{-3}
NaOH concentration	0.1 mol dm^{-3}
Mean linear flow rate of electroplating solution, v	8.0 cm s^{-1}
Kinematic viscosity of NaOH solution at 75 °C, ν	5.4×10^{-3} cm^2 s^{-1}
Channel Reynolds number, *Re*	≈ 710
Temperature, *T*	75 °C

Table 3. Charge transfer current ratios of the Pt/Ti mesh and Pt/Ti micromesh vs. a Pt/Ti plate (+ ITP) along their approximate A_e values for H electrosorption. The charge transfer-controlled current was recorded at η = –20.0 mV for the reduction of 0.1 mol dm^{-3} Ce(IV).

Electrode	Open-circuit potential *vs*. $Hg\|Hg_2SO_{4(sat.)}$, E_0 / mV	Current (charge transfer), I_{CT} / mA	Current ratio to Pt/Ti plate electrode + ITP, Ψ / dimensionless	Active electrode area for H adsorption, A_a / cm^2	Volumetric active electrode area for H adsorption, A_e / cm^{-1}
Pt/Ti plate + ITP	+883.5±2.9	–13.5±2.6	1.0	748.8±16.8	87.9±2.0
Pt/Ti mesh	+885.7±3.2	–65.3±13.7	4.8	≈ 3,600	≈ 190
Pt/Ti micromesh	+882.8±0.1	–113.1±2.3	8.4	≈ 6,300	≈ 1,010

Figure Captions

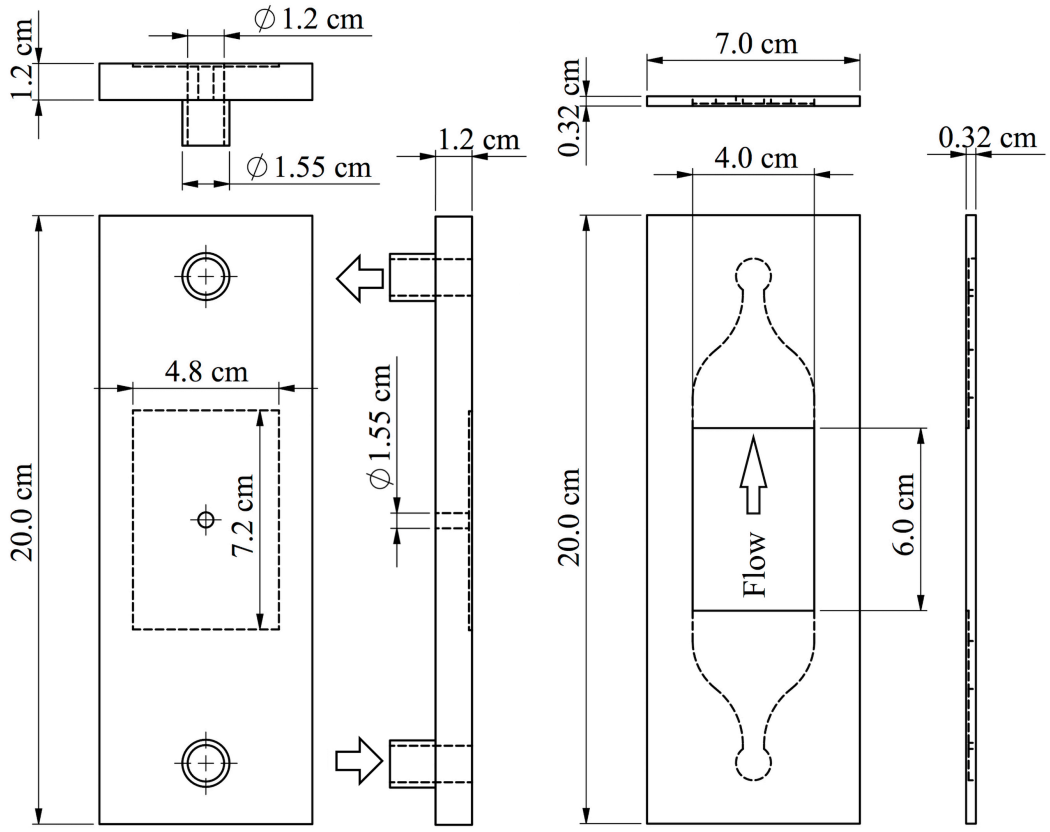

a) Electrode back plate b) Electrode flow channel frame

Figure 1. Acrylic polymer components of the negative half-cell of the rectangular channel flow cell employed during the electrodeposition of platinum. a) Electrode back plate; holds the planar current feeder of the micromesh stack (Figure 2a), a screw for electrical connection and electrolyte manifolds. b) Electrode flow channel frame; contains the micromesh stack and electrolyte flow. The components of the positive half-cell are symmetrical in respect to the ion exchange membrane.

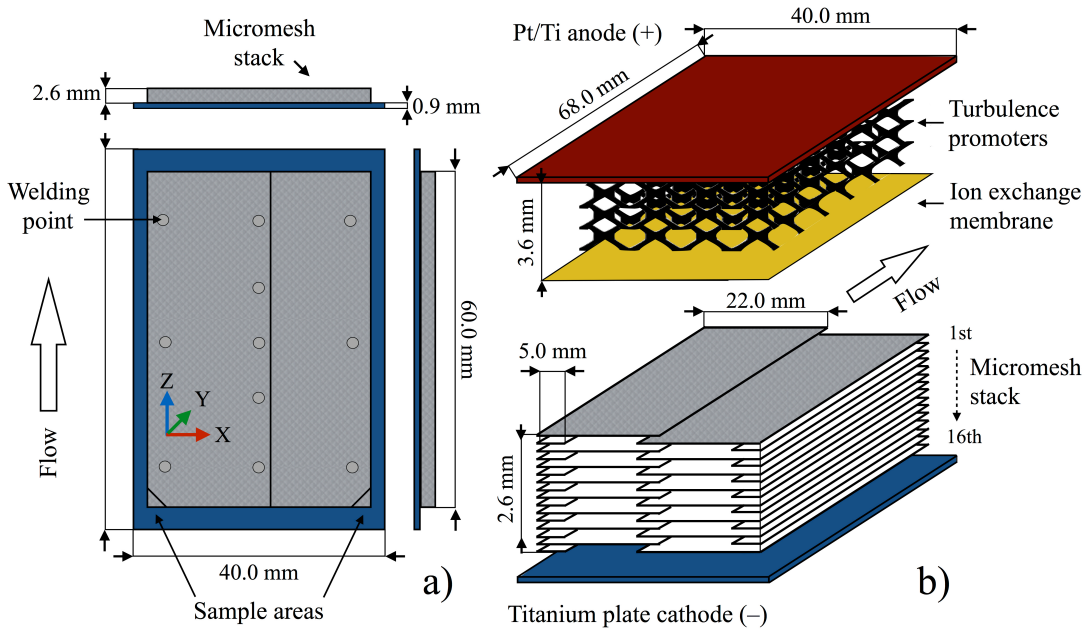

Figure 2. a) Disposition of the Pt/Ti micromesh stack electrode and its planar current feeder. b) Exploded view of the Pt/Ti micromesh stack cathode in the negative half-cell and the Pt/Ti plate anode in the positive half-cell as present the membrane-divided flow cell. The turbulence promoters within the positive half-cell are also shown. For clarity, polymer cell frames are omitted.

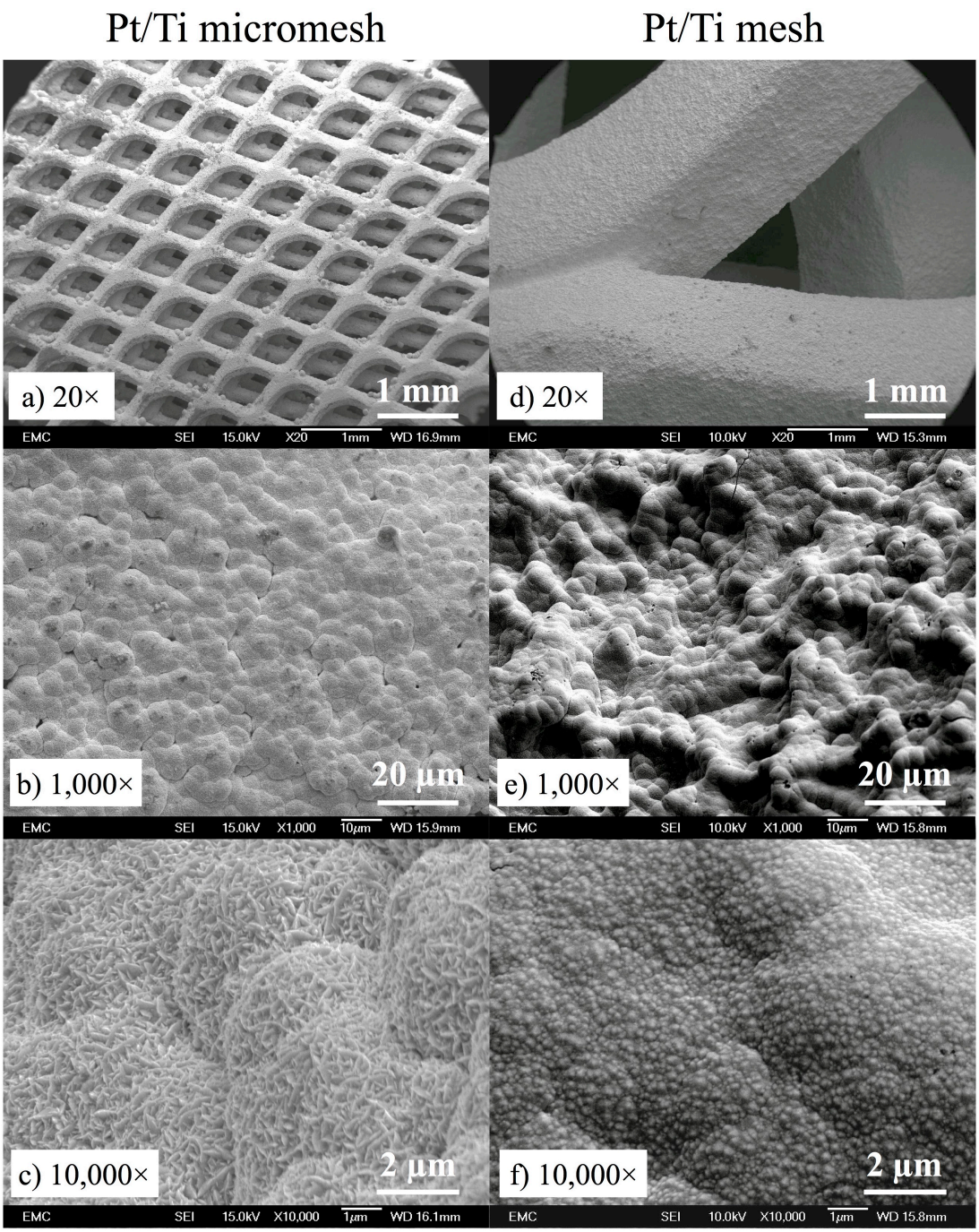

Figure 3. SEM images of the external surface: a) Pt/Ti micromesh and d) Pt/Ti mesh electrodes. In these images, the overall plating solution flow direction was from left to right along the observed planes during the electrodeposition. SEM images of the Pt-coated surfaces at higher magnification: b) Pt/Ti micromesh and e) Pt/Ti mesh. Microscopic appearance of Pt nucleation: c) Pt/Ti micromesh and f) Pt/Ti mesh.

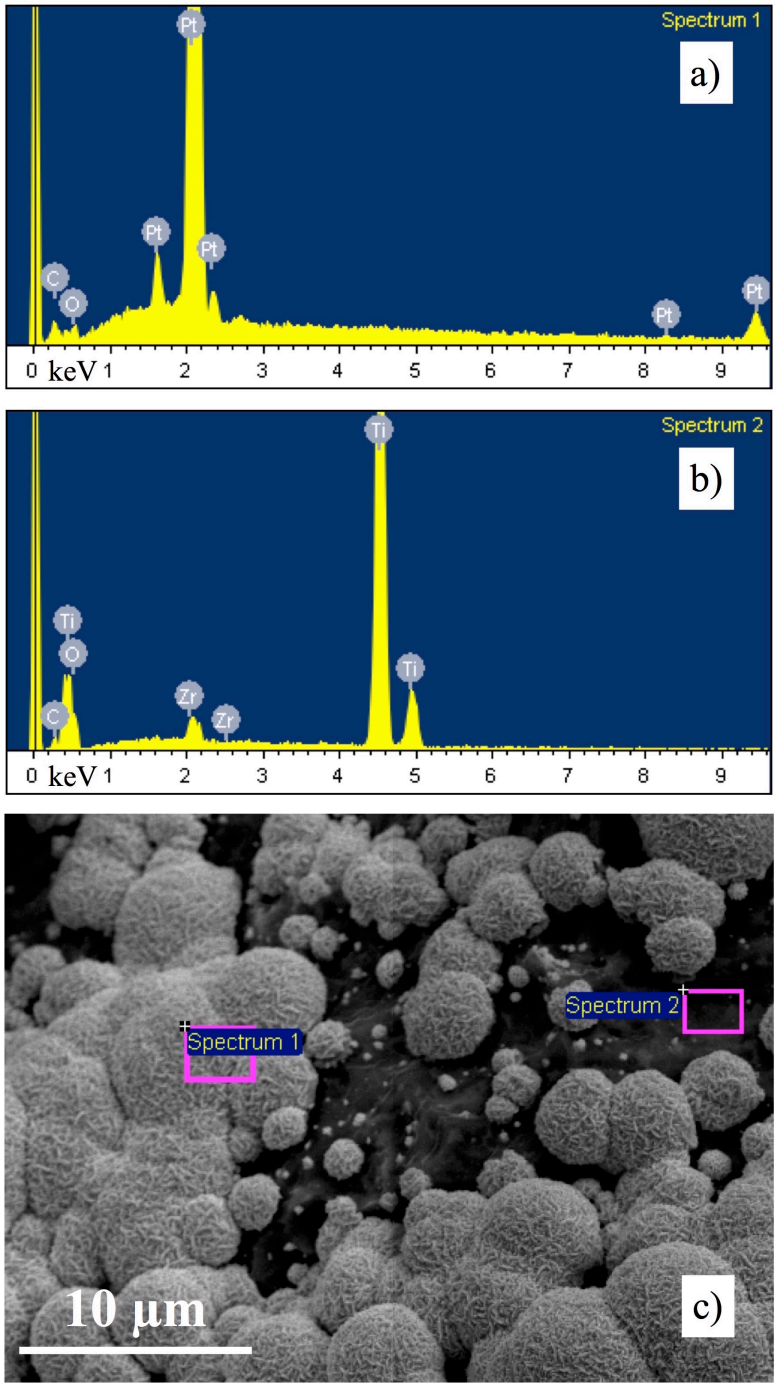

Figure 4. EDS elemental composition of Pt/Ti micromesh. a) platinum electrodeposit nucleated on the Ti, b) titanium substrate, c) SEM image of the analysed site.

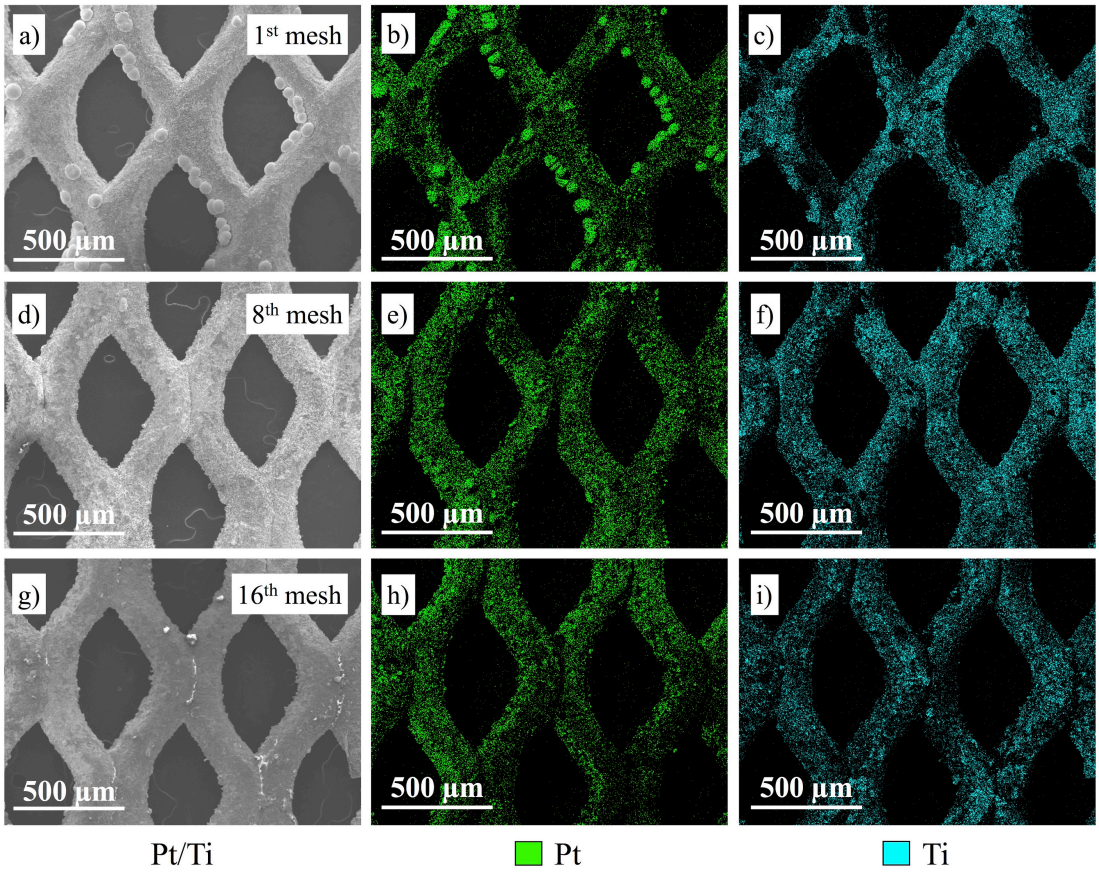

Figure 5. Platinum coating of individual meshes in the stack of Pt/Ti micromesh electrodes (following the Y axis). a), d), g) SEM images of 1st, 8th and 16th mesh, respectively. b), e), h) Platinum EDS mapping of 1st, 8th and 16th mesh, respectively (in green). c), f), i) Titanium EDS mapping of 1st, 8th and 16th mesh, respectively (in blue). The 1st mesh is adjacent to the membrane and the 16th is adjacent to the current feeder during electrodeposition. In these images, the overall plating solution flow direction was approximately from bottom to top along the observed planes.

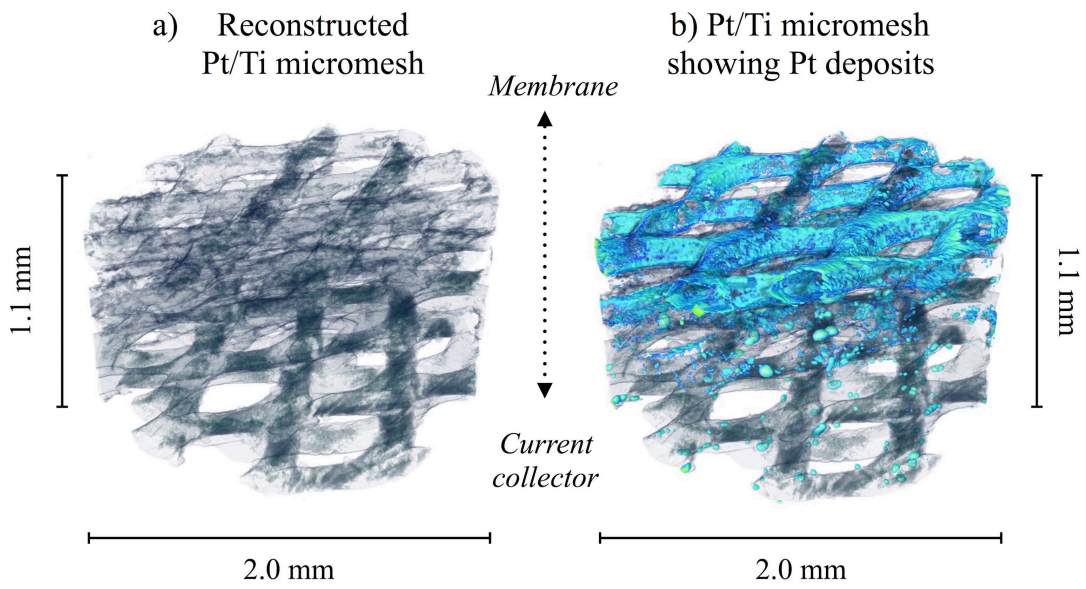

Figure 6. CT image of a cylindrical volume section of a) reconstructed Pt/Ti micromesh electrode and b) reconstructed Pt/Ti micromesh electrode showing an area with higher coverage of platinum (bright blue). The reconstructed electrode consisted of sections of the 1st, 2nd, 5th, 8th, and 16th meshes (in order of proximity to the membrane) embedded in epoxy resin. The vertical axis in the image represents the Y axis of the cell.

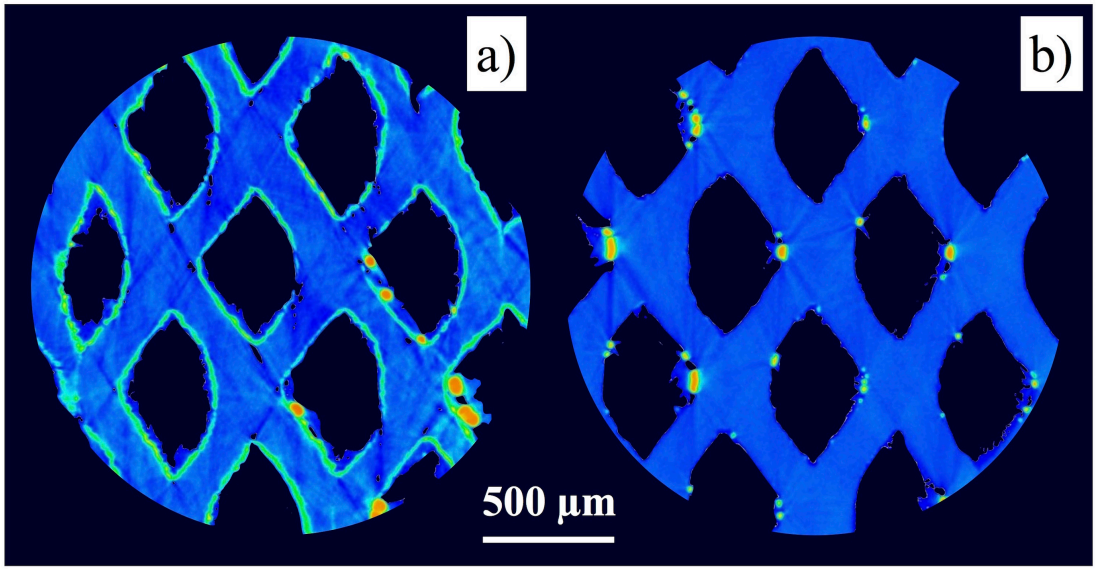

Figure 7. CT images of individual micromeshes part of the Pt/Ti micromesh electrode showing the platinum (bright green, yellow and red) coating on the titanium substrate (light blue). a) middle cross-section (X-Z plane) of the 1st micromesh, b) middle cross-section (X-Z plane) of the 16th micromesh, in order of proximity to the membrane. For clarity, contrast artefacts were digitally replaced with the background colour.

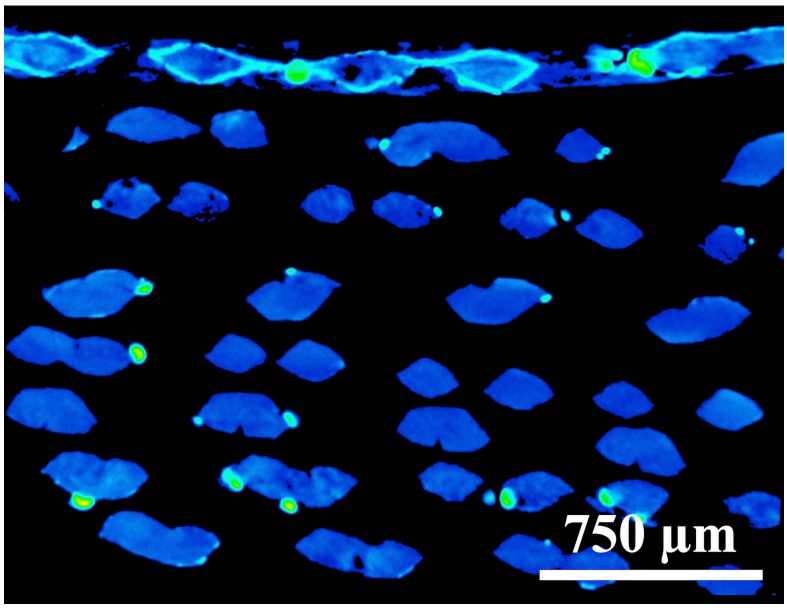

Figure 8. CT image of the cross section of a reconstructed Pt/Ti micromesh electrode indicating the platinum deposit distribution. The reconstructed electrode consisted of sections of the 1st, to 8th meshes (in order of proximity to the membrane) embedded in epoxy resin. Bright features are platinum, blue features are titanium, black is air. The vertical axis in the image represents the Y axis of the cell.

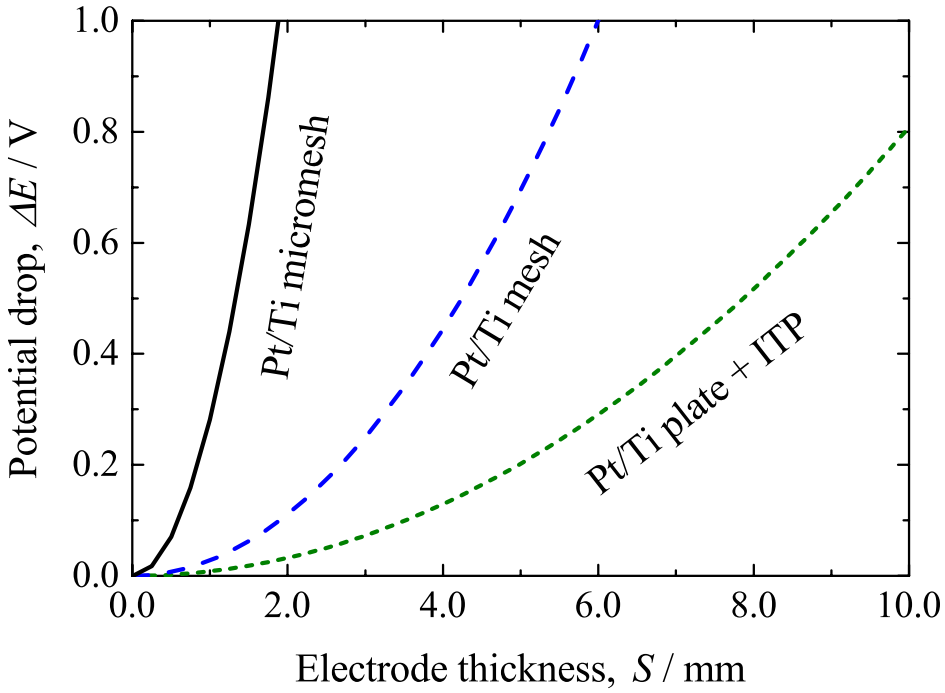

Figure 9. Potential drop within the electrolyte phase between the membrane and planar current feeder (Y axis) of various Pt/Ti electrodes at the cross-sectional plane at the entrance of a rectangular electrode channel during the reduction of Ce(IV) ions. The electrolyte properties correspond to a SOC of 50% in a Ce-based RFB. $k_m A_e$ values for the Pt/Ti micromesh, Pt/Ti mesh and Pt/Ti plate + ITP electrodes, are 0.055 s^{-1}, 5.4 × 10^{-3} s^{-1} and 1.6 × 10^{-3} s^{-1}, respectively [3]. The electrolyte contains 0.4 mol dm^{-3} Ce(IV) methanesulfonate and 0.4 mol dm^{-3} Ce(III) methanesulfonate in 4.0 mol dm^{-3} methanesulfonic acid. Its measured conductivity is 375 mS cm^{-1} [45].

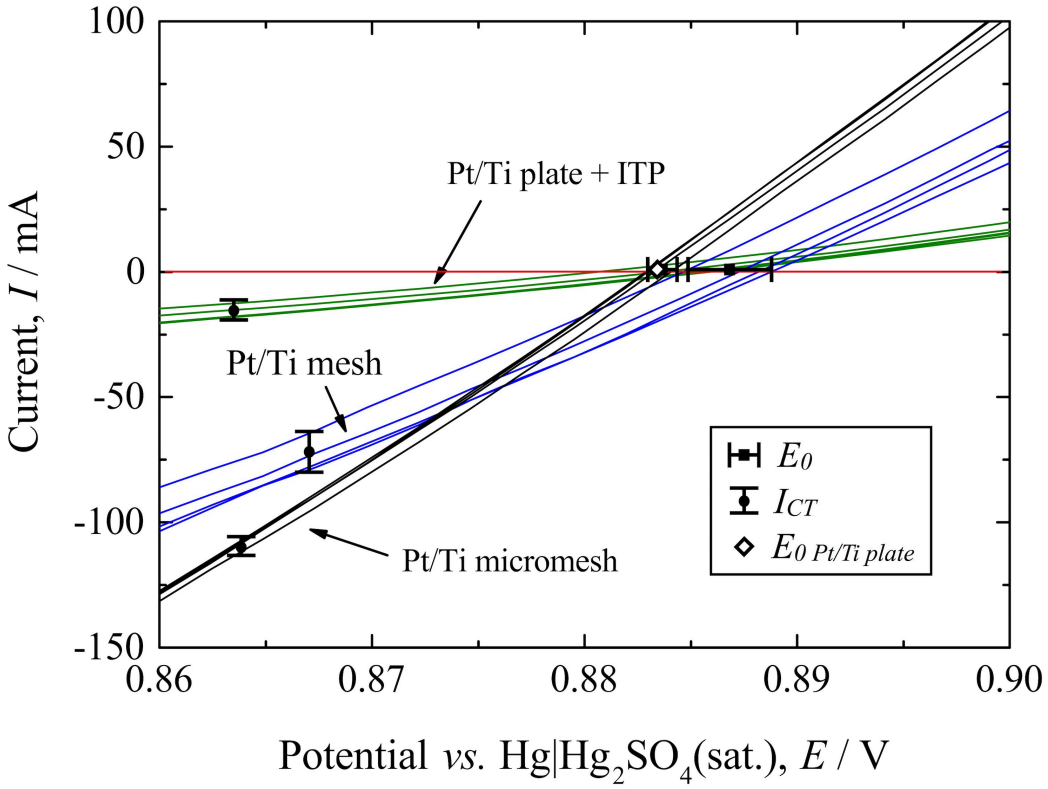

Figure 10. Linear sweep voltammetry of Pt/Ti micromesh, Pt/Ti mesh and Pt/Ti plate electrodes for the reduction of 0.1 mol dm^{-3} Ce(IV) at 25 °C showing the equilibrium potential, E_0, and charge transfer current at an overpotential of –20 mV for each electrode material.